# Small-angle X-ray scattering from sulphonated polyurethane ionomers based on toluene diisocyanate

**Y. Samuel Ding*, Richard A. Register, Chang-zheng Yang†, and Stuart L. Cooper‡**

*Department of Chemical Engineering, University of Wisconsin – Madison, Madison, WI 53706, USA*

*(Received 15 July 1988; accepted 1 September 1988)*

A series of sulphonated polyurethane ionomers based on poly(tetramethylene oxide), poly(propylene oxide), and polybutadiene (PTMO, PPO, and PBD) polyols was examined by small-angle X-ray scattering (SAXS). As the polyol molecular weight is increased, the ionic aggregate number density decreases and the aggregate size increases. PPO-based ionomers form smaller and more regularly spaced aggregates than do PTMO- or PBD-based ionomers. The limited data suggest that the aggregate size decreases with increasing valency. For PTMO-based materials neutralized with zinc and cadmium, increasing the temperature increased the fraction of ionic groups dissolved in the polymer matrix, especially for the zinc-neutralized sample. The degree of phase separation for these two samples paralleled the modulus–temperature trend.

**(Keywords: ionomer; polyurethane ionomer; small-angle X-ray scattering; morphology; aggregate dissociation temperature)**

## INTRODUCTION

In the preceding paper[1], we discussed the synthesis and thermomechanical characterization of a series of sulphonated polyurethane ionomers based on toluene diisocyanate (TDI) and either poly(tetramethylene oxide), poly(propylene oxide), or polybutadiene (PTMO, PPO, or PBD) polyols. The central morphological feature of these materials is that the ionic groups aggregate into microdomains, which act as physical crosslinks and impart elastomeric properties to the materials. However, direct observation of these ionic aggregates through electron microscopy has proved difficult[2]. Instead, small-angle X-ray scattering (SAXS) is generally used as a morphological probe[3–10]. SAXS is particularly well suited for the study of ionomers, because of the small size (2–10 nm) of the ionic aggregates and their high electron density relative to the polymer matrix, giving rise to a strong X-ray contrast. This paper describes the results of our SAXS investigations on the polyurethane ionomers discussed previously[1]. The variables studied included polyol type, polyol molecular weight, neutralizing cation, sample preparation method, and temperature. As before, the first character in the mnemonic sample code is the polyol type ('M' for PTMO, 'P' for PPO, and 'B' for PBD), the second character is the polyol molecular weight in thousands, and the last two characters are the cation's chemical symbol.

* Present address: Baxter Healthcare Corporation, Round Lake, IL 60073, USA

† Present address: Department of Chemistry, Nanking University. People's Republic of China

‡ To whom correspondence should be addressed

## EXPERIMENTAL

### *Sample preparation*

The synthesis of the polyurethane ionomers was described in the previous paper[1]. Samples for the SAXS experiments were generally prepared by spin-casting at 60°C from DMF solution (for polyether-based ionomers) or from a chloroform/methanol (5:1) mixture at 20°C (for the PBD-based ionomer). To examine the effect of sample preparation on morphology, some samples were also compression-moulded, and some were spin-cast from methanol at 25°C or tetrahydrofuran(THF)/water (5:1 v/v) solutions at 25°C.

### *SAXS measurements*

The small-angle X-ray scattering data were obtained using an Elliot GX-21 rotating anode generator, an Anton–Paar compact Kratky scattering camera, and a TEC model 211 linear position-sensitive detector. CuK$\alpha$ radiation was monochromatized using a nickel filter and pulse height discrimination. The scattering camera has a sample-to-detector distance of 60 cm and a detector length of approximately 8 cm, which provides a $q$ ($q = (4\pi/\lambda)\sin\theta$, where $2\theta$ is the scattering angle and $\lambda$ the wavelength of the radiation) range of 5.7 $nm^{-1}$, with a minimum $q$ of 0.15 $nm^{-1}$ due to the position of the beam stop. The detector length was divided into 128 channels for a resolution of $\approx 0.05\ nm^{-1}$. High temperature SAXS measurements were performed using a sample holder equipped with an Anton–Paar K-HR conduction hot stage and temperature controller.

The data were corrected for detector sensitivity, parasitic and background scattering, and absorption of

0032-3861/89/071213-08$03.00

X-rays by the sample. The beam profile along the slit length was measured and the iterative method developed by Lake[11] was used to desmear the data. Absolute scattering intensities expressed in terms of $I/I_eV$ were determined by comparing the sample scattering intensity to that from a calibrated Lupolen (polyethylene) standard[12]. Background scattering was determined by fitting the SAXS data in the high $q$ region using Porod's law[13] plus a constant background term.

## RESULTS AND DISCUSSION

All the SAXS data collected here exhibit two features commonly found in ionomer SAXS patterns: a peak, from 0.8 to 2.0 $nm^{-1}$ in $q$, and an upturn in scattered intensity at very low $q$, $<0.5\,nm^{-1}$. The 'ionomer' peak has been taken as evidence of ionic aggregation since it was first observed[3]. The origin of the upturn has been the source of considerable controversy, but recent investigations employing anomalous small-angle X-ray scattering[14] have suggested that it is related to an inhomogeneous distribution of ionic groups dissolved in the polymer matrix. In this paper, we will concern ourselves primarily with the peak. To analyse the SAXS data, we employed a modified version of the Yarusso–Cooper liquid-like interparticle interference model[5], which produces good fits to the ionomer peak[5,14] but does not reproduce the upturn. In this model, the ionic aggregates are modelled as monodisperse hard spheres with radius $R_1$; however, they are coated with a sheath of polymer, such that the radius of closest approach $R_2 > R_1$. The electron density of the aggregates is $\rho_1$, while those of the sheath and the polymer matrix are $\rho_0$. Originally, Yarusso used the Fournet[15] three-body type interference function, based on the Born–Green theory of liquid structure. However, Kinning and Thomas[16] have since shown that the Percus–Yevick total correlation function[17], as solved by Wertheim[18] and Thiele[19], provides a more satisfactory fit to the SAXS data from diblock copolymers exhibiting a spherical morphology. Thus, the Percus–Yevick function is expected to give better results for high ionic aggregate concentrations, where many-body effects become more important.

The equations describing the scattered intensity from this model are:

$$I/I_eV=(1/v_p)(4\pi R_1^3/3)^2(\rho_1-\rho_0)^2\Phi^2(qR_1)S(q) \quad (1)$$

where $v_p$ is the volume of material per ionic aggregate (inverse of aggregate number density), $I_e$ is the scattering from a single electron, $V$ is the scattering volume, and $\Phi$ is the scattering from a single sphere[20]:

$$\Phi(qR)=3[\sin(qR)-(qR)\cos(qR)]/(qR)^3 \quad (2)$$

$S(q)$ is the interference function, given in the Percus–Yevick form by

$$S(q, R_2, v_p, f)=[1+(12f)G(2qR_2)/qR_2]^{-1} \quad (3)$$

where

$$G(A)=(a/A^2)(\sin A-A\cos A) \quad (4)$$
$$+(b/A^3)[2A\sin A+(2-A^2)\cos A-2]$$
$$+(c/A^5)\{-A^4\cos A+4[3(A^2-2)\cos A$$
$$+(A^3-6A)\sin A+6]\}$$
$$a=(1+2f)^2/(1-f)^4 \quad (5)$$
$$b=-6f(1+f/2)^2/(1-f)^4 \quad (6)$$
$$c=f(1+2f)^2/2(1-f^4) \quad (7)$$
$$f=4\pi R_2^3/3v_p \quad (8)$$

Note that $f$ is the volume fraction of hard spheres. The modelling results, which are listed in *Tables 1, 3* and *4*, will be discussed below as the data are presented. Note that, in contrast to ionomers[10] based on PTMO and methylene bis(*p*-phenyl isocyanate), MDI, no pronounced high-$q$ shoulder on the ionomer peak was visible for the samples under discussion, even on a logarithmic intensity scale. Thus, the Yarusso model was able to produce a satisfactory fit in the ionomer peak region for all data examined.

### *Effect of polyol type*

For the best illustration of the effect of polyol type, consider the M2Na, P2Na, and B2Na materials, whose SAXS patterns are shown in *Figures 1* and *2*. These three materials are essentially identical in chain architecture except for the polyol type. The $q$ value at which the maximum occurs decreases in the order P2Na > M2Na ≈ B2Na. Since we attribute the scattering to interparticle interference, this indicates an increase in the average spacing between aggregates in the order B2Na ≈ M2Na > P2Na, which is reflected in the $v_p$ values in *Table 1*. This suggests that P2Na contains more ionic aggregates than M2Na or B2Na; the $R_1$ values also indicate that the aggregates in P2Na are smaller than in M2Na or B2Na, such that the level of phase separation is similar for the three materials.

Regarding the electron densities, $\rho_1-\rho_0$ decreases in the order B2Na > M2Na > P2Na. However, the electron densities of the polymer matrices are increasing in this same order. While accurate estimates of the matrix densities are difficult to compute, using density values of

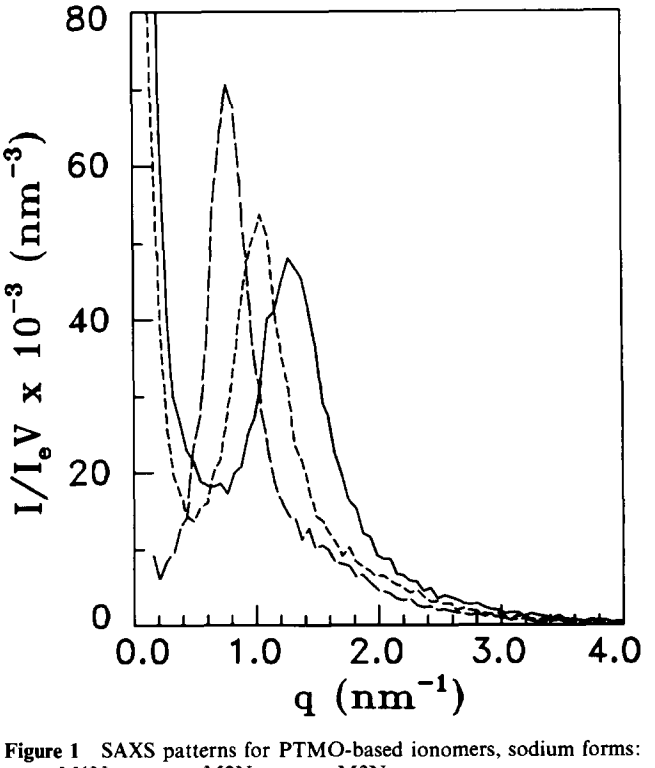


**Figure 1** SAXS patterns for PTMO-based ionomers, sodium forms: ——, M1Na; – – – –, M2Na; — —, M3Na

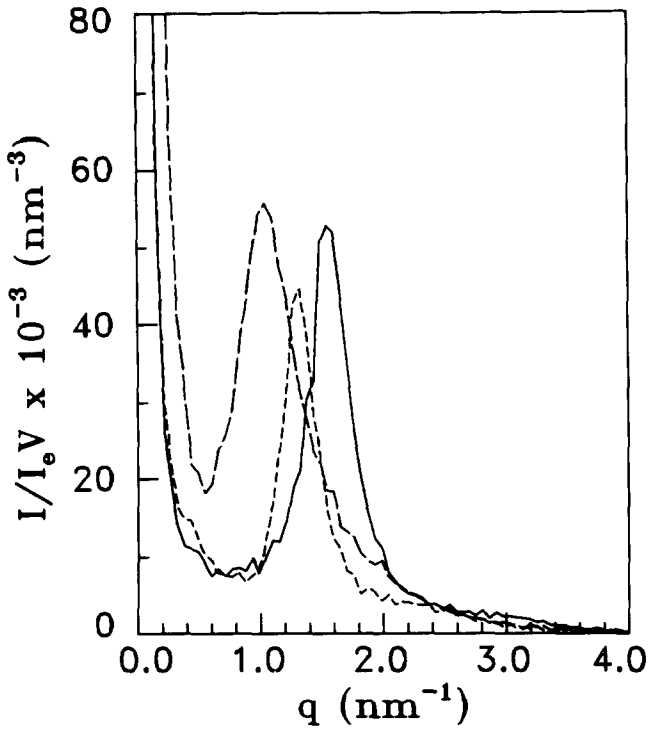


**Figure 2** SAXS patterns for PPO- and PBD-based ionomers, sodium forms: ——, P1Na; – – – –, P2Na; — —, B2Na

**Table 1** Model fit parameters at 25°C

| Sample[a] | $R_1$ (nm) | $R_2$ (nm) | $v_p$ (nm$^3$) | $\rho_1-\rho_0$ (nm$^{-3}$) |
|---|---|---|---|---|
| M1Na | 1.40 | 2.26 | 186 | 336 |
| M1Na[b] | 1.41 | 2.37 | 231 | 380 |
| M1Na[c] | 1.35 | 2.32 | 165 | 321 |
| M1Ca | 1.26 | 2.16 | 157 | 334 |
| M1Ni | 1.63 | 2.88 | 326 | 384 |
| M1Ni[d] | 1.15 | 2.25 | 174 | 570 |
| M1Zn | 1.36 | 2.37 | 235 | 417 |
| M1Zn[d] | 1.31 | 2.26 | 205 | 519 |
| M1Cd | 1.37 | 2.41 | 219 | 524 |
| M1Cs[d] | 1.97 | 1.31 | 467 | 485 |
| M1Eu | 0.99 | 1.93 | 121 | 507 |
| M2Na | 1.59 | 3.03 | 407 | 322 |
| M3Na | 1.92 | 3.99 | 878 | 283 |
| P1Na | 1.35 | 2.10 | 94 | 270 |
| P2Na | 1.37 | 2.53 | 161 | 251 |
| B2Na[e] | 1.48 | 2.84 | 372 | 380 |

[a] Cast from DMF solution at 60°C except where noted
[b] Cast from THF/water (5:1) solution at 20°C
[c] Compression-moulded at 180°C and 8000 psi (55 MPa)
[d] Cast from methanol at 20°C
[e] Cast from chloroform/methanol (5:1) solution at 20°C

0.89 g cm$^{-3}$ for PBD (value for amorphous sec-butyl lithium-initiated homopolymer[21]), 0.98 for PTMO (from Vallance and Cooper, for amorphous PTMO soft segments in segmented polyether-esters[22]), and 1.01 for PPO (for 2000 molecular weight oligomer, no ethylene oxide capping[23]), matrix electron densities of 297 (PBD), 327 (PTMO), and 335 $e^-$ nm$^{-3}$ (PPO) may be calculated. This indicates that the $\rho_1$ values are 677 (B2Na), 649 (M2Na), and 586 $e^-$ nm$^{-3}$ (P2Na). In other words, the electron densities of the aggregates are similar for all three materials, although that for P2Na appears lower, perhaps reflecting that the cations are less densely packed within the more numerous aggregates in P2Na. It should also be noted here that any fluctuation in incident X-ray intensity during data collection will reflect itself solely in the value of $\rho_1-\rho_0$.

Comparisons may also be made between the M1Na and P1Na materials, shown in *Figures 1* and *2*. Again, substantially lower values of $v_p$ and $R_1$ are found for the PPO-based material, suggesting that it has more numerous, but smaller, ionic aggregates. Note also that the average distance between particles, $v_p^{1/3}$, is approximately equal to the closest approach distance $2R_2$ for the PPO ionomers (4.55 *versus* 4.20 nm for P1Na, 5.44 *versus* 5.06 nm for P2Na). This indicates a comparatively regular packing of the ionic aggregates, which may be seen directly in the SAXS data by the sharpness of the peak compared with PTMO- or PBD-based materials. Modelling the data with a paracrystalline model[24], with disorder of the second kind, also indicates a relatively low disorder in comparison with the PTMO- or PBD-based ionomers[25].

*Effect of polyol molecular weight*

SAXS curves for the PTMO-based ionomers M1Na, M2Na, and M3Na are shown in *Figure 1*. As the polyol molecular weight increases, the peak moves to lower $q$ and the value of $v_p$ increases, as expected. The $R_1$ values increase with polyol molecular weight as well, as does the thickness of the polymer sheath ($R_2-R_1$). This observation contrasts with that made by Yarusso[5] for sulphonated polystyrene (SPS) ionomers, where the $R_1$ and $R_2$ values were found to be essentially independent of sulphonation and neutralization levels. However, the ionic groups in SPS are placed randomly along the polymer backbone, whereas in the polyurethane ionomers the ionic groups are spaced at regular intervals, which could produce larger and more regularly spaced ionic aggregates.

Comparisons may also be made between the P1Na and P2Na materials, whose SAXS data are shown in *Figure 2*. The same trends are found here, although there is little difference in the $R_1$ values between the two materials.

*Effect of sample preparation method*

To examine the effect of sample preparation, samples of the M1Na ionomer were compression-moulded at 180°C and 8000 psi (55 MPa) and cast from a THF/water (5:1) solution, as well as from DMF. The SAXS curves for these three samples are shown in *Figure 3*. While the SAXS patterns are largely similar, as expected, sample morphology does appear to change slightly with preparation method. The aggregate sizes, as measured by $R_1$ and $R_2$, are essentially identical for all three preparation methods. However, the $v_p$ values increase in the order compression-moulded < DMF cast < THF/water cast. Since the ion content is the same for all three samples, and $R_1$ varies little among them, the increasing values of $v_p$ suggest an increasing number of ionic groups dissolved in the matrix[5,14]. Ions are most likely to remain dispersed, or 'trapped', in the matrix if the solvent from which the sample was cast has a high polarity; compression- moulding may be viewed as 'casting' from the polymer matrix material, PTMO in this case. Since polarity increases in the order PTMO < DMF < THF/water, it seems logical that the number of dissolved ions and the values of $v_p$ should increase in the same way.

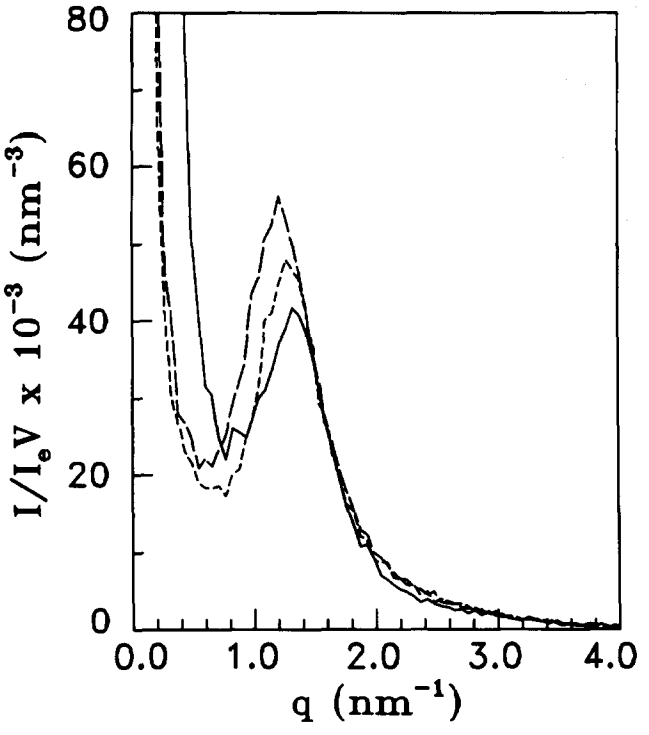


**Figure 3** SAXS patterns for M1Na: ——, compression-moulded, – – – –, cast from DMF at 60°C; — —, cast from THF/water (5:1) at 20°C

Similar trends were noted in the preceding paper[1] by dynamic mechanical analysis, where the M1Na material cast from THF/water had a lower rubbery plateau modulus than the same material cast from DMF. The decrease in modulus was attributed to dissolved ionic groups, which decrease the physical crosslink density.

The values of $\rho_1 - \rho_0$ also increase in the same order as the $v_p$ values. The higher electron density contrast for the THF/water cast sample is surprising, since water has an electron density comparable to that for the matrix material; therefore, any residual water left in the ionic aggregates should lower, not raise, the electron density contrast. We currently have no explanation for this observation.

The effect of casting solvent on the M1Ni and M1Zn materials was also examined, casting from both DMF and methanol. The SAXS patterns are shown in *Figure 4*, and here the choice of casting solvent has a marked effect on the morphology. Examining the Yarusso model parameters in *Table 1* shows that casting from methanol produces smaller ($R_1$), less numerous ($v_p$), and more densely packed ($\rho_1 - \rho_0$) aggregates than does casting from DMF. The last observation also serves to explain why casting M1Zn from methanol produces a material with a higher modulus than does casting from DMF, as noted in the previous paper[1]. A higher electron density difference implies closer packing of the cations, which further suggests that the Coulombic interactions holding the aggregate together will be stronger and that ionic groups cannot be removed from the aggregate as easily. This then inhibits stress-relaxation by 'ion-hopping', leading to a higher modulus, as discussed in the previous paper[1]. This emphasizes the importance of casting solvent on both morphology and properties for the polyurethane ionomers. On the other hand, when M1Ni is cast from DMF or methanol, materials of similar moduli are produced, even though the aggregate electron density is different. However, M1Ni already has the lowest $\alpha_c$ value of any material in the M1 series, indicating that ion-hopping is effectively eliminated over the time scale of the test, regardless of which casting solvent is used. Therefore, further increases in aggregate cohesion do not result in changes in the mechanical properties.

*Effect of cation type*

The neutralizing cation was found to have an appreciable effect on the morphology of the ionomers, although it was not as important as the polyol type or molecular weight. The SAXS patterns for M1Na (*Figures 1* and *3*), M1Ni and M1Zn (*Figure 4*), M1Eu, M1Ca and M1Cd (*Figure 5*), and M1Cs and M1Ag (*Figure 6*) exhibit clear differences. With the exception of M1Ag, all exhibit clear ionomer peaks indicative of a well ordered morphology. M1Ag, on the other hand, exhibits only a weak ionomer peak as a shoulder on very intense low-$q$ scattering. Because of the difficulty in separating the peak from the upturn, we did not attempt to model the ionomer peak in M1Ag. However, the qualitative features of its SAXS pattern merit further discussion. The shape of the SAXS pattern is reminiscent of those observed by Galambos *et al.*[26] for a manganese-neutralized sulphonated polystyrene (MnSPS) ionomer. Upon quenching from THF/water solution, MnSPS exhibited no ionomer peak, but the peak developed as the sample was heated above 160°C. This was interpreted as a transition from an unaggregated system in the quenched state to an aggregated system upon annealing. A similar argument suggests that the M1Ag material exhibits very poor phase separation. The strength of the low-angle scattering in M1Ag is also remarkable. As mentioned above, recent investigations by anomalous small-angle X-ray scattering (ASAXS) suggest that the upturn arises from an inhomogeneous distribution of dissolved ionic groups in the material[14].

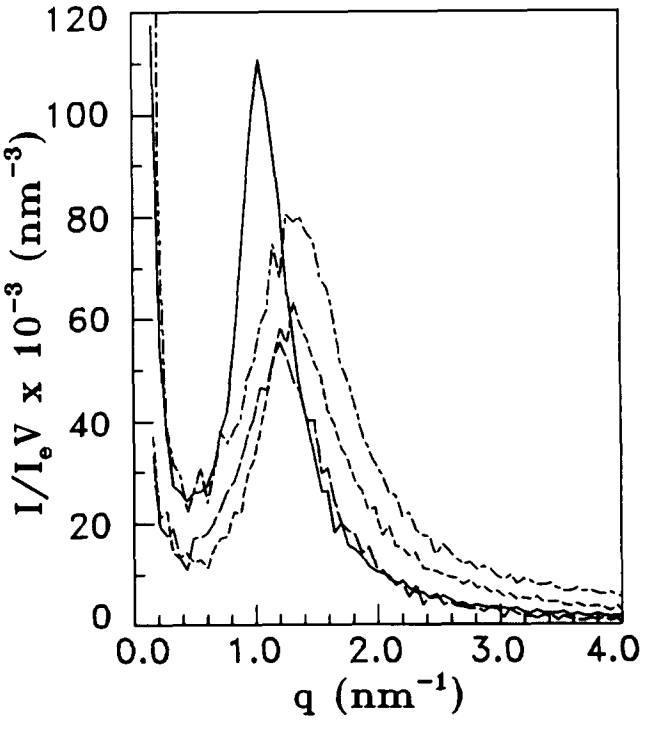


**Figure 4** SAXS patterns for: ——, M1Ni cast from DMF; – – – –, M1Ni cast from methanol; — —, M1Zn cast from DMF; — – —, M1Zn cast from methanol

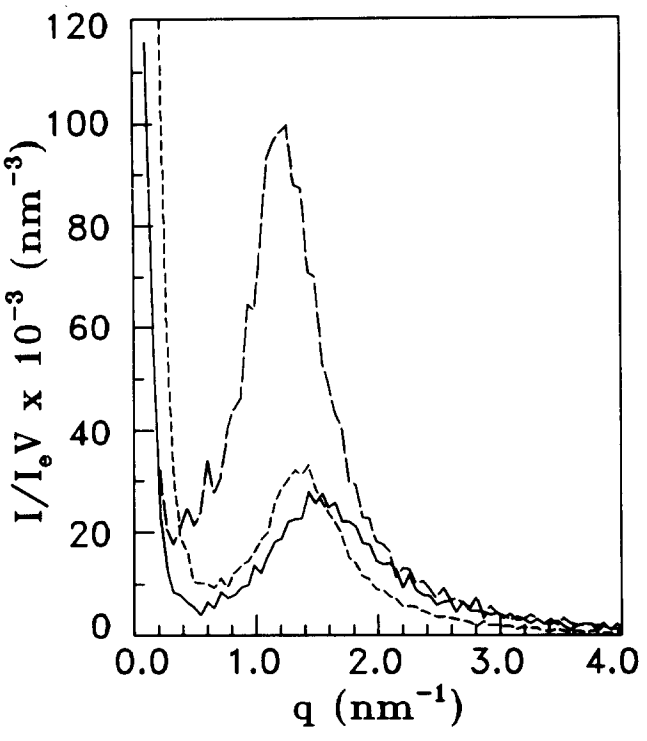


**Figure 5** SAXS patterns for the PTMO-1000 based ionomers with different cations: ——, M1Eu; – – – –, M1Ca; — —, M1Cd

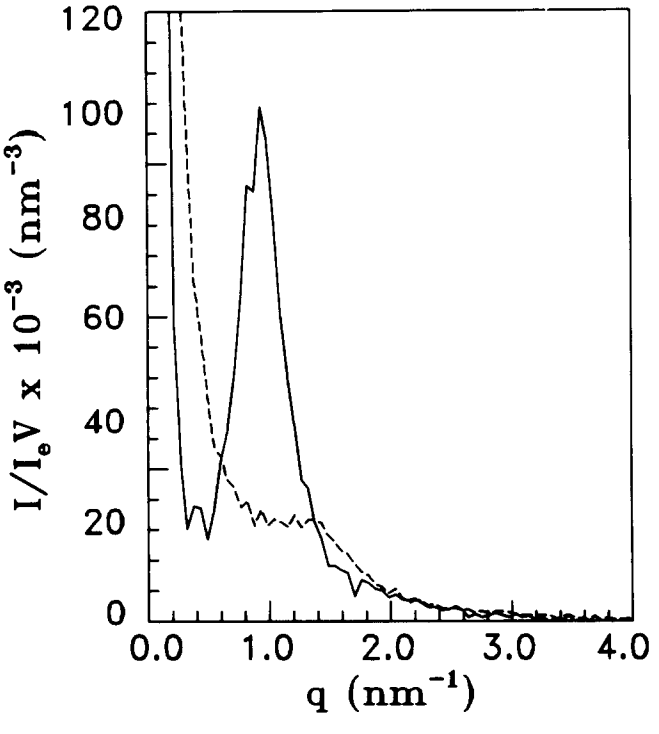


**Figure 6** SAXS patterns for the PTMO-1000 based ionomers with different cations: ——, M1Cs; – – – –, M1Ag

Therefore, the intensity of the upturn would be expected to increase with the fraction of dissolved ionic groups, and therefore increase at the expense of peak intensity. This effect may also be seen in the data of Galambos *et al.*, and will be discussed below with regard to our high temperature investigations.

Turning to the Yarusso model fit parameters listed in *Table 1*, it may be seen that most of the $R_1$ values lie in the relatively narrow range 1.26–1.63 nm, with the trivalent $Eu^{3+}$ cation producing an $R_1$ value of only 0.99 nm, and the large monovalent $Cs^+$ cation attaining 1.97 nm. While the data are sparse, it seems that the average aggregate size decreases with increasing valency. This may be understood by considering the possible packing arrangements within the aggregate. The cations must be balanced by a number of sulphonate groups equal to their valency, and in general these sulphonate groups will come from different polymer chains or from widely spaced groups on the same chain. Simply to maintain charge neutrality, then, the number of possible configurational arrangements of the polymer chains is reduced compared with the non-ionic case, and this restriction becomes more severe with increasing cation charge. Further packing the cations together into aggregates results in an even greater restriction on the number of conformations available to the chains, and thus it may be expected that the less severe restriction (smaller entropy loss) present when cations of lower valency are used will lead to a state wherein the ionic aggregates are larger (greater release of Coulombic energy, hence lower enthalpy).

The $R_2 - R_1$ values lie in the range 0.86–1.31, and generally increase with $R_1$. Since larger aggregates will necessarily require the attachment of greater numbers of polymer chains, this trend is not unexpected. The $v_p$ values increase with $R_1$; since the ion content, as measured by the density of sulphonate groups, is the same for all M1 materials, the parallel trends in $v_p$ and $R_1$ simply reflect that, if the aggregates are larger, there must be fewer of them. The $v_p$ values range from 121 (M1Eu) to 467 nm$^3$ (MiCs), a nearly fourfold change in the number density of ionic aggregates. This effect may be seen directly in the SAXS patterns as well, since the peak position occurs at largest $q$ for M1Eu and at smallest $q$ for M1Cs.

The trends in the $\rho_1 - \rho_0$ values are also interesting. As may be observed from the intensities of the SAXS patterns, the electron density contrast generally increases with atomic number $Z$. However, for cations of similar $Z$, the contrast would be expected to be lower for materials containing cations of higher valency $u$, since the aggregates must then contain more of the less-electron-dense sulphonate groups and fewer cations. Therefore, as a first approximation, $\rho_1 - \rho_0$ should be expected to increase monotonically with $Z/u$. This approximation is rather crude, as it completely ignores the differences in packing that are likely to be encountered with cation, as shown in the crystal structures of low molecular weight compounds. However, the $\rho_1 - \rho_0$ values, and the intensities of the SAXS patterns, do indeed increase regularly with $Z/u$, as shown in *Table 2*, with the glaring exception of M1Cs. Compared with the other materials in *Table 2*, $Cs^+$ gives an electron density contrast that is much lower than expected, indicating that the cations within the aggregates are very loosely packed. In a subsequent paper[27] on these materials, we show by extended X-ray absorption fine structure (EXAFS) spectroscopy that this is indeed the case. Note that the difference should not be due to the fact that M1Cs was cast from methanol while the others were cast from DMF; the $\rho_1 - \rho_0$ values in *Table 1* show that, for M1Ni and M1Zn, casting from methanol produces ionic aggregates with a higher electron density than does casting from DMF.

**Table 2** Electron density differences for the M1 series[a]

| Sample | $\rho_1-\rho_0$ (nm$^{-3}$) | Atomic number $Z$ | Atomic number/cation charge $Z/u$ |
|---|---|---|---|
| M1Ca | 334 | 20 | 10 |
| M1Na | 336 | 11 | 11 |
| M1Ni | 384 | 28 | 14 |
| M1Zn | 417 | 30 | 15 |
| M1Cs[b] | 485 | 55 | 55 |
| M1Eu | 507 | 63 | 21 |
| M1Cd | 524 | 48 | 24 |

[a] Cast from DMF at 60°C, except where noted
[b] Cast from methanol at 20°C

One final point of interest is that while SAXS indicates that appreciable variation in morphology can be induced by varying the cation, neither $R_1$ nor $v_p$ seems to correlate with the physical property trends observed in the preceding paper[1]. This suggests that neither the size nor the number density of the ionic aggregates controls the physical properties. Further discussion on this point will also be presented in a subsequent paper[27].

*High temperature measurements*

It has been proposed on thermodynamic grounds that a critical temperature should exist for ionic aggregate dissociation[28]. However, no such temperature has yet been observed. High temperature SAXS experiments were conducted on PTMO-1000 based polyurethane ionomers neutralized with divalent zinc and cadmium (M1Zn and M1Cd) in the hope of observing such a transition. Zinc was chosen because of its relatively covalent bonding nature, which causes the ionic aggregates in zinc-neutralized ionomers to be relatively labile[29], as reflected in the greater degree of 'ion-hopping' discussed in the preceding paper[1]. Cadmium was chosen because it lies below zinc in the periodic table, and so may or may not give rise to behaviour similar to that found with zinc.

*Figures 7* and *8* show the SAXS curves, on logarithmic scales, for M1Cd and M1Zn heated from 25°C to 220–225°C. Model fit parameters for each curve are listed in *Tables 3* and *4*. The SAXS pattern, and implicitly the morphology, of M1Cd changes little with temperature. The dashed line in the figure is centred on the ionomer peak in the SAXS pattern at 25°C, and visual inspection shows that the peak position moves only slightly upon heating. A slight broadening and decrease in the peak intensity occurs above 200°C, which is reflected in the increase in $v_p$; this suggests that some of the ionic aggregates have dissociated. However, the general similarity of the SAXS patterns in *Figure 7* indicates that most of the aggregates in M1Cd maintain their integrity upon heating to at least 220°C.

The results for M1Zn are qualitatively different, as shown in *Figure 8*. Above 175°C, the peak moves sharply to lower $q$, indicating that the average spacing between ionic aggregates increases. The model fit parameters in *Table 4* also indicate that the size of the aggregates, as measured through $R_1$, increases; however, the volume fraction of ionic aggregates $g$, equal to $4\pi R_1^3/3v_p$, decreases. These observations indicate that, above 175°C, both coalescence and dissociation of the ionic aggregates are occurring, but the net result is that more ionic groups are dispersed in the matrix at higher temperatures.

For both the M1Zn and M1Cd samples, the $\rho_1-\rho_0$ values remain relatively constant as the temperature is increased. Assuming that the aggregates have a much lower coefficient of thermal expansion than the matrix, as would be expected for largely inorganic material, and that the aggregate internal structure does not change with temperature, the only change in the contrast factor would be due to the thermal expansion of the PTMO matrix

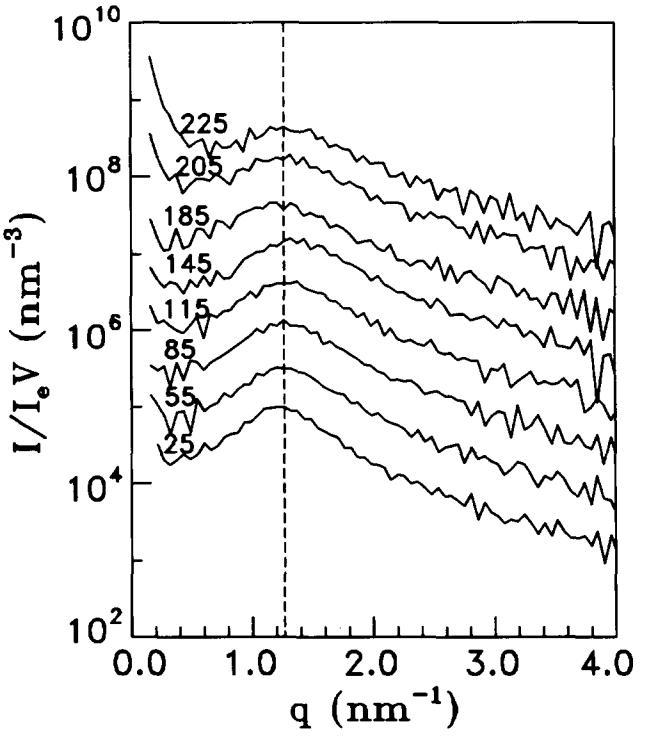


**Figure 7** SAXS patterns for M1Cd at elevated temperatures. Numbers indicate the temperature in °C. Each curve beyond 25°C has been successively shifted by 0.6 units on the log scale for clarity

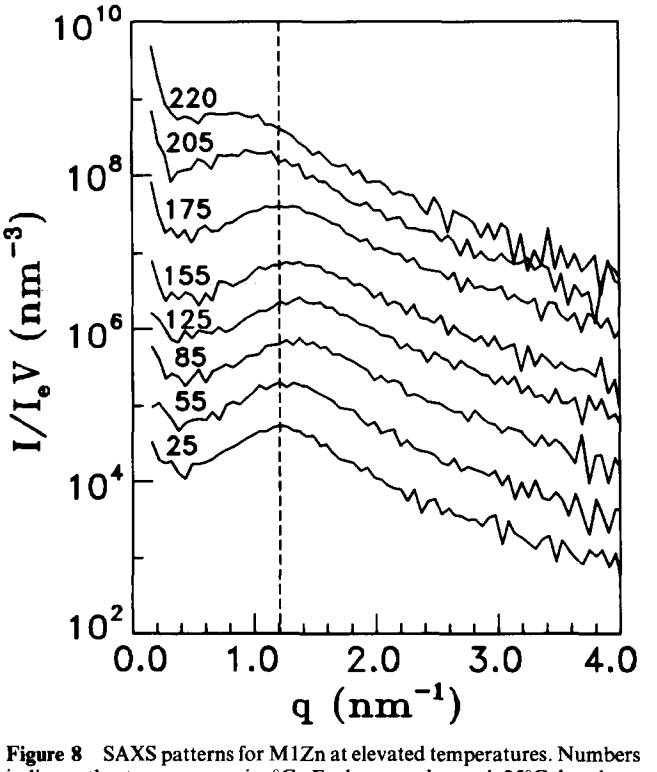


**Figure 8** SAXS patterns for M1Zn at elevated temperatures. Numbers indicate the temperature in °C. Each curve beyond 25°C has been successively shifted by 0.6 units on the log scale for clarity

**Table 3** Model fit parameters for M1Cd at different temperatures

| $T$ (°C) | $R_1$ (nm) | $R_2$ (nm) | $v_p$ (nm$^3$) | $\rho_1-\rho_0$ (nm$^{-3}$) | $g^a$ |
|---|---|---|---|---|---|
| 25 | 1.37 | 2.41 | 219 | 524 | 0.049 |
| 55 | 1.28 | 2.31 | 209 | 565 | 0.042 |
| 85 | 1.25 | 2.30 | 205 | 584 | 0.040 |
| 115 | 1.21 | 2.25 | 203 | 585 | 0.037 |
| 145 | 1.18 | 2.17 | 171 | 552 | 0.040 |
| 185 | 1.14 | 2.06 | 167 | 487 | 0.037 |
| 205 | 1.18 | 2.22 | 244 | 509 | 0.028 |
| 225 | 1.17 | 2.10 | 236 | 451 | 0.028 |

[a] $g=4\pi R_1^3/3v_p$, volume fraction of ionic aggregates

**Table 4** Model fit parameters for M1Zn at different temperatures

| $T$ (°C) | $R_1$ (nm) | $R_2$ (nm) | $v_p$ (nm$^3$) | $\rho_1-\rho_0$ (nm$^{-3}$) | $g^a$ |
|---|---|---|---|---|---|
| 25 | 1.36 | 2.37 | 235 | 417 | 0.045 |
| 55 | 1.28 | 2.26 | 212 | 453 | 0.041 |
| 85 | 1.19 | 2.11 | 177 | 487 | 0.040 |
| 125 | 1.14 | 2.06 | 167 | 485 | 0.037 |
| 155 | 1.16 | 2.13 | 193 | 448 | 0.034 |
| 175 | 1.24 | 2.25 | 254 | 490 | 0.031 |
| 205 | 1.48 | 2.65 | 559 | 484 | 0.024 |
| 220 | 1.63 | 3.10 | 1052 | 438 | 0.017 |

[a] $g=4\pi R_1^3/3v_p$, volume fraction of ionic aggregates

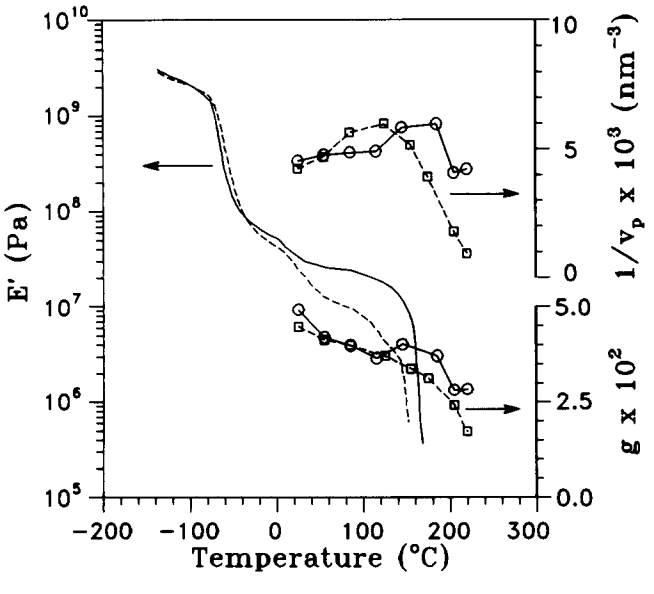


**Figure 9** DMTA data for (——) M1Cd and (– – – –) M1Zn, number density of ionic aggregates ($1/v_p$) and volume fraction of ionic aggregates $g$. ○, M1Cd; □, M1Zn

material. Based on linear expansion coefficient of $1.6\times10^{-4}$ determined by Schneider and Paik Sung[30] for PTMO oligomer, a decrease of about 9% in the matrix density would be expected over this temperature range, leading to an increase of approximately $29\,e^-$ nm$^{-3}$ in $\rho_1-\rho_0$. However, this approximation assumes that the aggregates are composed of purely ionic material, whereas the absolute $\rho_1-\rho_0$ values indicate they must contain a substantial fraction of less-electron-dense organic material or water. (For comparison, anhydrous $CdSO_4$ has an electron density of $1301\,e^-$ nm$^{-3}$ at room temperature.) Thermal expansion of the organic material in the aggregates will tend to reduce the changes in electron density contrast from the $29\,e^-$ nm$^{-3}$ calculated above. The observed $\rho_1-\rho_0$ values for M1Zn and M1Cd show no apparent trend, and are 463 and $532\,e^-$ nm$^{-3}$, with standard deviations of 28 and $48\,e^-$ nm$^{-3}$, respectively. We feel that the variation in these values reflects the fluctuation in incident X-ray intensity during the course of the experiment. Since the standard error for the M1Cd sample is 9%, this may explain the unexpected higher electron density contrast, by 13%, observed for M1Na when cast from THF/water instead of DMF, as discussed above.

For both samples, the ionomer peak position moves to slightly higher $q$ on heating from 25 to about 150°C (for M1Zn) or 180°C (for MiCd). Examining the liquid model parameters, we see that $v_p$ and $R_1$ decrease over the same interval. This suggests that the slight shift of peak position is primarily due to a redistribution of ions between aggregates, as these samples (originally cast from DMF) attain the equilibrium bulk morphology for the temperature of observation. It should be noted that these changes are larger for M1Zn than for M1Cd; as discussed in the preceding paper, the covalent bonding nature of $Zn^{2+}$ produces relatively labile aggregates. However, for both samples, the changes below 170°C are much smaller than those observed above 170°C. This is shown in *Figure 9*, where the number density of ionic aggregates, $1/v_p$, and the volume fraction of ionic aggregates $g$, are plotted against temperature along with the DMTA storage modulus curves taken from the preceding paper. As the temperature is increased, the $g$ values for M1Cd initially decrease, in parallel with $E'$, and then flatten out. Above 200°C, the $g$ values decrease again; at this temperature, the material has lost most of its elasticity and has become a viscous liquid, as the $E'$ curve shows. Most of the increased mobility of the polymer chains at elevated temperature is due primarily to 'ion-hopping', that is, most of the ions remain in aggregates at any given instant, but transport of ions between aggregates becomes easier with increasing temperature[31–33]. However, the SAXS results show that the volume fraction of ionic aggregates decreases at the highest temperatures, indicating that more ions are dispersed in the matrix. For M1Zn, $g$ decreases monotonically with temperature, exhibiting no plateau, as does the storage modulus. However, the rate of decrease in $g$ increases markedly when the material has entered the viscous flow region. Again this indicates that at high temperatures, more ionic groups become dispersed in the matrix.

For both M1Zn and M1Cd, the scattered intensity at very low $q$ increases with temperature. If the upturn is indeed due to dissolved ionic groups, as discussed above, then the intensity of the low $q$ scattering would be expected to increase with the fraction of dissolved ionic groups. Since the $g$ values decrease at high temperatures, this is exactly what is observed. It should also be noted that the low $q$ intensity, as shown in *Figures 7* and *8*, increases most dramatically for M1Zn above 150°C and for M1Cd above 180°C, which coincides with the changes in $v_p$ and $g$ discussed above.

## CONCLUSIONS

Sulphonated polyurethane ionomers have been used to study the effects of polyol molecular weight (ion content), polyol type (polymer matrix type), sample preparation

method, neutralizing cation, and temperature on ionomer morphology. SAXS measurements and modelling indicate that as the polyol molecular weight is increased, the aggregate number density decreases and the aggregate size increases. PPO-based ionomers form smaller and more regularly spaced ionic aggregates than do PTMO- or PBD-based ionomers. The polarity of the casting solvent can alter the morphology slightly by changing the fraction of ionic groups dispersed in the polymer matrix. The choice of neutralizing cation has an appreciable effect on the morphology of the material; the limited data acquired here suggest that the size of the ionic aggregates decreases with cation valency. The M1Ag sample exhibited unusually poor phase separation compared with samples differing only in cation type. Studying the SAXS patterns of M1Zn and M1Cd as a function of temperature revealed that as temperature is increased, more ionic groups are dispersed in the polymer matrix. The effect is more noticeable for M1Zn than for M1Cd, due to the more labile nature of ionic aggregates containing $Zn^{2+}$, and increases most strongly when the materials are in the viscous flow region. The degree of phase separation paralleled the trends in $E'$ measured by DTMA, confirming that the lower $E'$ observed for M1Zn is due to a lower density of elastically effective chains.

## ACKNOWLEDGEMENTS

The authors acknowledge partial support of this research by the US Department of Energy (DE-FG02-84-ER45111) and the Division of Materials Research of the National Science Foundation (DMR 86-03839). R.A.R. wishes to thank the Fannie and John Hertz Foundation for financial support while this work was completed.

## REFERENCES

1 Ding, Y. S., Register, R. A., Yang, C.-z. and Cooper, S. L. *Polymer* 1989, **30**, 1204
2 Handlin, D. L., MacKnight, W. J. and Thomas, E. L. *Macromolecules* 1981, **14**, 795
3 Wilson, F. C., Longworth, R. and Vaughan, D. J. *ACS Div. Polym. Chem. Polym. Prepr.* 1968, **9**, 505
4 Marx, C. L., Caulfield, D. F. and Cooper, S. L. *Macromolecules* 1973, **6**, 344
5 Yarusso, D. J. and Cooper, S. L. *Macromolecules* 1983, **16**, 1871
6 Yarusso, D. J. and Cooper, S. L. *Polymer* 1985, **26**, 371
7 Fujimara, M., Hashimoto, T. and Kawai, H. *Macromolecules* 1981, **14**, 1309
8 Weiss, R. A. and Lefelar, J. A. *Polymer* 1986, **27**, 3
9 Williams, C. E., Russell, T. P., Jérôme, R. and Horrion, J. *Macromolecules* 1986, **19**, 2877
10 Lee, D.-c., Register, R. A., Yang, C.-z. and Cooper, S. L. *Macromolecules* 1988, **21**, 998
11 Lake, J. A. *Acta Cryst.* 1967, **23**, 191
12 Kratky, O., Pilz, I. and Schmitz, P. J. *J. Colloid Interface Sci.* 1966, **21**, 24
13 Porod, G. *Kolloid Z.* 1951, **124**, 83
14 Ding, Y. S., Hubbard, S. R., Hodgson, K. O., Register, R. A. and Cooper, S. L. *Macromolecules* 1988, **21**, 1698
15 Fournet, P. G. *Acta Crystallogr.* 1951, **4**, 293
16 Kinning, D. J. and Thomas, E. L. *Macromolecules* 1984, **17**, 1712
17 Percus, J. K. and Yevick, G. *Phys. Rev.* 1958, **110**, 1
18 Wertheim, M. S. *Phys. Rev. Lett.* 1963, **10**, 321
19 Thiele, E. *J. Chem. Phys.* 1963, **39**, 424
20 Rayleigh, Lord *Proc. Roy. Soc. Lond.* 1914, **A90**, 219
21 Stempel, G. H. in 'Polymer Handbook', 2nd edn (Eds J. Brandrup and E. H. Immergut), Wiley, New York, 1975
22 Vallance, M. A. and Cooper, S. L. *Macromolecules* 1984, **17**, 1208
23 Arco Chemical, Thanol PPG-2000 Polyol Product Data, 1988
24 Hosemann, R. and Bagchi, S. N. 'Direct Analysis of Diffraction by Matter', North-Holland, Amsterdam, 1962
25 Ding, Y. S. *Ph.D. thesis*, University of Wisconsin – Madison, 1986
26 Galambos, A. F., Stockton, W. B., Koberstein, J. T., Sen, A., Weiss, R. A., Russell, T. P. *Macromolecules* 1987, **20**, 3091
27 Ding, Y. S., Register, R. A., Yang, C.-z. and Cooper, S. L. *Polymer* 1989, **30**, 1221
28 Eisenberg, A. *Macromolecules* 1970, **3**, 147
29 Bagrodia, S., Wilkes, G. L. and Kennedy, J. P. *Polym. Eng. Sci.* 1986, **26**, 662
30 Schneider, N. S. and Paik Sung, C. S. *Polym. Eng. Sci.* 1977, **17**, 73
31 Ward, T. C. and Tobolsky, A. V. *J. Appl. Polym. Sci.* 1967, **11**, 2903
32 Sakamoto, K., MacKnight, W. J. and Porter, R. S. *J. Polym. Sci. A-2* 1970, **8**, 277
33 Hara, M., Eisenberg, A., Storey, R. F. and Kennedy, J. P. in 'Coulombic Interactions in Macromolecular Systems', (Eds A. Eisenberg and F. E. Bailey), *ACS Symp. Ser.* 1986, **302**